Journal of Magnetism and Magnetic Materials 540 (2021) 168447

Contents lists available at ScienceDirect

Journal of Magnetism and Magnetic Materials

journal homepage: www.elsevier.com/locate/jmmm

Research articles

# Schottky-like anomaly in the heat capacity and magnetocaloric effect of charge-ordered single-crystalline (Sm, Ca, Sr)$MnO_3$ compound

Dipak Mazumdar [a,*], Kalipada Das [b], I. Das [a]

[a] CMP Division, Saha Institute of Nuclear Physics, HBNI, 1/AF, Bidhannagar, Kolkata 700064, India
[b] Department of Physics, Seth Anandram Jaipuria College, 10, Raja Naba Krishna Street, Kolkata 700005, India

ARTICLE INFO

*Keywords:*
Charge-ordered manganites
X-ray photoelectron spectroscopy
Magnetic phase diagram
Clausius–Clapeyron equation
Maxwell's relation
Schottky-like anomaly

ABSTRACT

We present a comprehensive experimental study on the magnetic and magnetocaloric properties of a charge-ordered single-crystalline $Sm_{0.5}Ca_{0.25}Sr_{0.25}MnO_3$ compound. The studies on x-ray photoelectron spectroscopy (XPS) reveals the presence of an equal distribution of $Mn^{3+}$ and $Mn^{4+}$ ions in the studied system. The Oxygen, O1s-core level spectra have been simulated with three binding energies curves, which correspond to the $O^{2-}$ ions, $O^{1-}$ ions, and chemically adsorbed oxygens, $O^{chem}$. The XPS analysis of the O1s-core-level spectra and magnetic characterizations indicate the proper stoichiometry of the present sample. Considering the change of volume phase fraction in the isofield magnetization measurements during the first-order magnetic phase transition from paramagnetic state to ferromagnetic state, the isothermal magnetic entropy change ($\Delta S$) has been estimated based on the modified Clausius–Clapeyron equation. An inverse magnetocaloric effect has also been noticed in the -$\Delta S$ vs. T plot calculated by Maxwell's thermodynamic relation, suggesting the dominant antiferromagnetic ground state supported by a charge-ordered phase of the studied system. The high-temperature zero-field heat capacity ($C_P$) data can be well-interpreted quantitatively using the Debye model of heat capacity. With the extracted magnetic heat capacity ($C_{mag}$) data, the temperature variation of the magnetic entropy (S(0)), as well as the adiabatic temperature change ($\Delta T_{ad}$), have been estimated. In addition to that, the low-temperature $C_P$ data displays a Schottky-like anomaly in the temperature region between 2 K and 20 K. The experimental data points are successfully fitted by considering the various contributing factors of the low-temperature heat capacity such as the lattice-phonon vibration ($C_{lat}$), antiferromagnetic spin-wave ($C_{mag}$), and the two-level Schottky function ($C_{sch}$) due to the energy splitting of the $Sm^{3+}$ cations.

## 1. Introduction

From the half of the century, both doped and undoped perovskite manganite compounds get massive importance at the forefront of condensed-matter physics research activity on account of their widespread applications in the area of magnetic switches, magnetic memory storage devices as well as in magnetic refrigerant cooling industries [1–7]. Generally, undoped $RMnO_3$ (R is trivalent elements, basically the lanthanides) compounds possessed antiferromagnetic (AFM) insulating properties [8,9]. Upon doping of R-site by any divalent elements (e.g. Ca, Sr, Ba, Pb, etc.), induces $Mn^{4+}$ ions in the $RMnO_3$ systems, which favors some fascinating inherent physical properties like charge-orbital ordering (COO), ferromagnetism, Jahn–Teller lattice distortion, metal–insulator like transition (MIT), which are leading to get colossal magnetoresistance (CMR), and large magnetocaloric effect (MCE) [10–16]. Due to the potential applications as well as to understand the rudimentary physics, investigations on CMR and MCE on manganite compounds have been widely carried out [10–16].

The change of isothermal magnetic entropy ($\Delta S$) and adiabatic temperature ($\Delta T_{ad}$) upon application of any external magnetic field is known as the MCE of any magnetic material [17]. Both the high values of $\Delta S$ and $\Delta T_{ad}$ along with negligible thermal and field hysteresis are the basic requirement for any refrigerant material in the magnetic cooling industries. Higher values of $\Delta S$ can be obtained in the vicinity of the magnetic phase transition temperature regions. In the case of doped perovskite manganite having the general formula $R_{1-x}A_xMnO_3$ (A is a divalent element), the doping concentration, x plays a vital role to achieve various magnetic ground states in manganite compounds like charge-ordered (CO) state, frustrated spin state, fully ferromagnetic (FM) or AFM state, and so on [18–25]. Charge-ordering is the checkerboard-like real-space ordering of $Mn^{3+}$ and $Mn^{4+}$ cations due to the predominant effect of onsite Coulomb repulsion energy over the kinetic energy of $e_g$ electrons and this phenomenon is generally observed for half-doping concentration (x = 0.5) in case of the doped manganite

* Corresponding author.
*E-mail address:* dipak.mazumdar@saha.ac.in (D. Mazumdar).

https://doi.org/10.1016/j.jmmm.2021.168447
Received 5 March 2021; Received in revised form 13 July 2021; Accepted 19 August 2021
Available online 28 August 2021

compounds [26–30]. Due to the equal distribution of $Mn^{3+}$ and $Mn^{4+}$ ions ($Mn^{3+}$: $Mn^{4+}$ = 1:1) in CO state, the $e_g$ electrons could not easily hope to its nearest neighbors and as a result, an insulating (AFM in nature) ground state is formed below the specific charge-ordered temperature ($T_{CO}$) [31,32]. Microscopically, all the spin, lattice, charge and orbital degrees of freedom play simultaneously in the CO-state and make this state a hot topic among the researchers [30]. The robustness of the CO state can be weaken upon application of external perturbations like magnetic field [33,34], electric field [4], pressure [35,36], radiation [37], etc. where, AFM-insulating ground state converted into an FM-metallic (FMM) state. Such a huge destabilization of the CO state leads to CMR and large MCE.

The classical Maxwell's thermodynamic relation (MR) [38] of the form

$$\Delta S = \int_0^H (\partial M/\partial T) dH \quad (1)$$

has been employed to estimate the change of magnetic entropy in most of the cases. A small change in the value of magnetization in the vicinity of magnetic phase transition could result in a higher value of $\Delta S$. The applicability of MR is suitable for a continuous magnetic phase transition region, which is second-order in nature [39]. However, for phase-separated systems like CO compounds, high possibility of having a meta-magnetic like phase transition, which is of the first-order in nature and accompanied by both thermal and field hysteresis. In this scenario, the application of MR to estimate the value of $\Delta S$ is not recommended due to the contradictory results obtained from both experimental and theoretical investigations [40–43]. This discrepancy may be arisen due to the conversion of the non-equilibrium nature of the volume phase fractions. To resolve this issue, Giguere et al. had advised to use the Clausius–Clapeyron (CC) equation [43] of the form,

$$\Delta S = -\Delta M \left(\frac{dH}{dT_c}\right) \quad (2)$$

rather than MR to calculate the $\Delta S$ associated with the first-order magnetic phase transition (FOPT). The direct application of MR in a FOPT system leads to a 'spike' in the $\Delta S(T)$ curve whose magnitude is far above the theoretically expected value and the underlying physics is still mysterious for researchers [44–46]. Recently, we have shown the reliability of CC equation to calculate the $\Delta S$ value in $Eu_{0.55}Sr_{0.45}MnO_3$ compound, having short-range FM interaction below T < 30 K and compared the value of $\Delta S$ as calculated by using the MR equation [47]. Similar kind of analysis of magnetic entropy change has also been reported for some intermetallic compounds [48,49].

In the family of manganites, $Sm_{0.5}Ca_{0.5}MnO_3$ compound carries notable importance due to the presence of its CO state with $T_{CO} \sim 250$ K [50,51]. This robustness of CO state can be melted upon application of a high magnetic field, H = 60 Tesla at 4.2 K [52]. But upon half doping of Ca-site by Sr-ions would help to reduce the critical magnetic field for destabilizing the CO-state up to 4.8 Tesla at $T = 2$ K, resulting in CMR of the order of $10^{15}$%, as reported by Banik et al. [53]. To understand the magnetic ground state of $Sm_{0.5}Ca_{0.25}Sr_{0.25}MnO_3$ (SCSMO) compound, we have constructed the magnetic phase diagram of the single-crystalline SCSMO compound both in-plane and out-of-plane configurations using the MCE as an effective tool as described in our earlier report [33]. Interestingly, the anisotropic nature of the magnetic ground state of SCSMO compound has been observed [33]. Lack of attention has been paid in the numerical value of $\Delta S$ in the vicinity of the magnetic phase transition region. One would also expect a Schottky-like anomaly in the low-temperature heat capacity data of a CO manganite compound. In this high CMR SCSMO compound, in-depth analysis of low-temperature heat capacity has not been carried out in earlier studies [33,53]. Less interest has also been paid in the study of low-temperature heat capacity of Sm-based manganite compounds.

Considering those contexts, we have chosen the single-crystalline form of the SCSMO sample for the present study. The primary aim of the present study is to explore the influence of the first-order nature of the magnetic phase transition on its MCE. In addition to that, we have also focussed our attention on the temperature-dependent heat capacity data of the sample especially at the low-temperature region, where different competing magnetic phases coexist together. Our experimental results indicate that the compound exhibits a moderate value of magnetocaloric parameters namely $\Delta S$, relative cooling power (RCP) and $\Delta T_{ad}$. The zero-field low-temperature heat capacity data shows a Schottky-like anomaly and this Schottky behavior is understood with two-levels Schottky function of heat capacity for $Sm^{3+}$ ions in a wide temperature scale of 2–42 K. The high-temperature heat capacity data has been analyzed with the help of the Debye model for lattice specific heat. In addition to that, we also performed the x-ray photoelectron spectroscopy (XPS) measurements to ensure the ratio of $Mn^{3+}$ and $Mn^{4+}$ ions which play an important role in case of the CO manganite compounds.

## 2. Experimental details

The single-crystalline SCSMO compound was prepared by conventional solid-state reaction method, followed by using a four-mirror-based float zone furnace (Crystal System Co.) [33]. Phase purity and crystal structure was confirmed for the as-cast powdered SCSMO compound from the x-ray diffraction pattern recorded at room temperature. The SCSMO compound was formed in single-phase, supported by the orthorhombic crystal symmetry with space group *Pnma* [33]. To investigate the immaculacy, chemical composition and oxidation states of the elements present in a sample, XPS is used as a very sensitive powerful tool. Here, we have used a monochromatic Al-$K_\alpha$ source with energy 1486.7 eV in an ultra-high vacuum XPS set-up from VG-SCIENTA. The binding energies were edited by neutral C-1s peak, which is assigned the value of 284.6 eV. For the evaluation of the XPS data, CASA-XPS software has been utilized. The Shirley background correction was employed to deconvolute the experimental curves with optimum minimizing the number of peaks used to well fit them. Both temperature and magnetic field dependence of magnetization measurements have been carried out using a vibrating sample magnetometer-based superconducting quantum interference device (SQUID-VSM, Quantum Design). Zero field heat capacity ($C_P$) measurements have been performed in a physical property measurement system (Quantum Design, USA) by relaxation technique.

## 3. Results and discussions

### 3.1. XPS study

A full survey scan of the SCSMO sample surface has been presented in Fig. 1(a). The XPS survey scan has confirmed the presence of Samarium (Sm), Calcium (Ca), Strontium (Sr), Manganese (Mn), and Oxygen (O) elements in the system. There is no foreign material present in the sample. It is decided from the absence of any other additional lines related to the contamination or impurity, except a peak at ~ 285 eV that corresponds to C-1s. This carbon (C-1s) peak may be attributed due to the residual carbon from the sample or adventitious hydrocarbon from the XPS instrument itself [54]. In manganite compounds, magnetic ordering is mainly attributed to the exchange mechanism between valence states of manganese ions. The well-fitted high-resolution XPS core level binding energy spectrum of the Mn-$2p_{3/2}$ region has been shown in Fig. 1(b). From Fig. 1(b), it has been observed that the Mn-$2p_{3/2}$ peak is mainly deconvoluted into two peaks at 641.48 eV and 642.80 eV which are corresponding to $Mn^{3+}$ and $Mn^{4+}$ ions respectively [55–58]. This decomposition of the main peak into two peaks indicates the coexistence of two oxidation states of Mn-ions. To calculate the relative fraction of the $Mn^{3+}$ and $Mn^{4+}$ cations in the sample, the area under

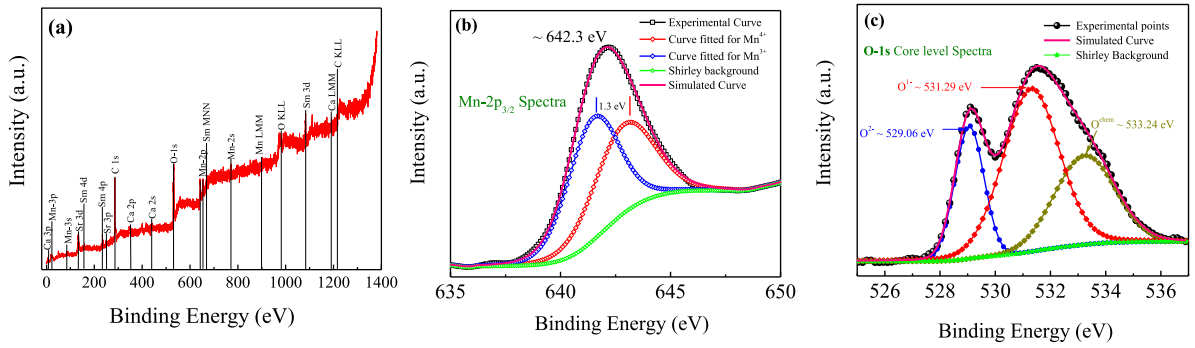


**Fig. 1.** (a) A full-range survey scan of the surface of SCSMO compound, (b) The deconvoluted XPS core-level spectra of Mn-2p lines in the Mn $2p_{3/2}$ spectral region. The blue curve is fitted for $Mn^{3+}$-ions and the red one is fitted for $Mn^{4+}$-ions. The pink curve overlapping with experimental data points is the as simulated curve and the bottom green curve is the as deducted Shirley Background curve, (c) The deconvoluted XPS core-level spectra of the O-1s peak. The fitted blue, red, and dark yellow curves are attributed to the $O^{2-}$-ions, $O^{1-}$-ions and chemically adsorbed oxygens, $O^{chem}$ respectively. (For interpretation of the references to color in this figure legend, the reader is referred to the web version of this article.)

**Table 1**
Various parameters evaluated during the fitting of the Mn-$2p_{3/2}$ core-level spectra.

| Peaks | Position (eV) | FWHM (eV) | Area under the curve |
|---|---|---|---|
| $Mn^{3+}$ | 641.48 | 2.38 | 518.89 |
| $Mn^{4+}$ | 642.80 | 3.03 | 501.31 |

**Table 2**
Different parameters obtained from the fitting of O-1s core-level spectra.

| Peaks | Position (eV) | FWHM (eV) | Area under the curve |
|---|---|---|---|
| $O^{2-}$ | 529.06 | 1.24 | 369.22 |
| $O^{1-}$ | 531.29 | 2.38 | 913.81 |
| $O^{chem}$ | 533.24 | 2.58 | 514.95 |

the $Mn^{3+}$ and $Mn^{4+}$ curves are utilized. The mixed-valence manganese ratio of $Mn^{3+}/Mn^{4+}$ in the present case is ~ 1.035, a generic feature of any CO manganite compound [56,58]. The peak positions, full-width at half-maximum (FWHM), area under the curves are listed in Table 1. Oxygen nonstoichiometry can also affect the relative proportion of the Mn-ions to maintain the electroneutrality [59]. In case of the CO SCSMO compound, the experimentally obtained $Mn^{3+}/Mn^{4+}$ is very close to 1, which suggests that our sample has almost stoichiometric oxygen content. The fitted Mn-$2p_{3/2}$ spectrum provides one of the vital information of the average valence states of Mn-ions present in the studied system. Following the procedure similar to the analysis as proposed by Wu et al. we have estimated the average valence state of Mn-ions and the obtained value is +3.491 [60].

Since, various contradictory reports have been found in the literature on O-1s peak of manganite systems, it is hard to accurately explain the O-1s peak [60–68]. Though we had tried to best fit the narrow scanned region of the O-1s spectrum and explained it with the help of literature. The core-level spectrum for binding energies of O-1s for SCSMO is presented in Fig. 1(c). After removing the background, using a Shirley background-type, the O-1s core level spectrum is fitted using three Gaussian curves. The binding energies are determined as 529.06 eV, 531.29 eV and 533.24 eV. The peak at 529.06 eV is attributed to the lattice oxygen in the form of $O^{2-}$ ions originated from the metal oxides present in the sample, which provides the information about the hybridization of O-2p with transition metal ions (basically Mn-O bonds) [60,63,66,67]. The intermediate peak at 531.29 eV can be linked with the oxygen vacancies i.e. the oxygen-related defects due to the surface adsorbed oxygen or hydroxyl species or other radical, such as CO or $CO_2$, in the oxygen-deficient regions in the sample [54,63]. But for the present scenario, it is almost impossible to have the oxygen vacancy in the studied system due to the following reasons: (a) the photoelectrons of the O-1s spectra originated from the 1s electrons of oxygen atom. The vacancy without atoms cannot emit the photoelectrons, (b) According to the fitted result of Fig. 1(c), the oxygen vacancy content is more than the lattice oxygen content which is impossible to form a crystal structure. Hence, the intermediate peak at 531.29 eV of O-1s spectra is attributed to the presence of $O^{1-}$ ions that could allow the compensation for some deficiencies in the subsurface of the transition-metal oxides [60,66–68]. This fact is also supported by the work carried out by Wu et al. where they had showed that the peak intensity was decreasing with the increment of the oxygen vacancy content [68]. The higher binding energy peak observed at 533.24 eV indicates loosely bound oxygen, from chemically adsorbed water molecules on the surface, $O^{chem}$ of the sample [60,64–66]. All the fitted parameters like peak-position, FWHM and area under the curves obtained from the fitting of O-1s core-level spectra are listed in Table 2.

To find out the average valence state of oxygen ions in the present system, we have considered the area under the curves corresponding to $O^{2-}$ and $O^{1-}$ ions respectively [60,67,68]. The estimated average valence of the oxygen ion, $V_{aO^-}$ is −1.712, which is in good agreement with the already reported values found in the Refs. [60,67,68] and also the references therein. To get the charge neutrality for any stable compound, the absolute values of the anion valance should be equal to the sum of all the cation valences ($V_{aC^+}$) present in the system [68]. For any oxide-based compound having the general formula $ABO_{3-\delta}$ ($\delta$ is used to represents the excess or lack of oxygen content), one can find out the actual oxygen content of the sample using the relation $(3-\delta)|V_{aO^-}| = V_{aC^+}$ and the obtained value of $\delta$ is −0.49. Therefore, the oxygen content in the present sample is more than 3.

### 3.2. Magnetization study

To understand the magnetic ground state of the SCSMO system, isothermal magnetization (M–H) measurements have been performed at $T$ = 5 K, 50 K and 150 K as shown in Fig. 2(a). Before each measurement, the system along with the sample is cooled down to the desired temperature from room temperature in absence of any magnetic field. Linear increment of magnetization with the magnetic field at $T$ = 5 K supports the AFM ground state of the compound at low field values. At a critical magnetic field of $H_C$ ~ 2.7 Tesla at T = 5 K, the system undergoes a meta-magnetic-like transition (AFM → FM). This change of magnetization is irreversible in nature and the system remains in the FM state after subsequent field cycling [33]. The presence of strong magnetic field hysteresis at $T$ = 50 K is pointing towards the fact of coexistence of multiple magnetic phases in the system [47]. This kind of S-shaped magnetization curves along with field hysteresis is a clear signature of having FOPT in the system [69]. Absence of any magnetic

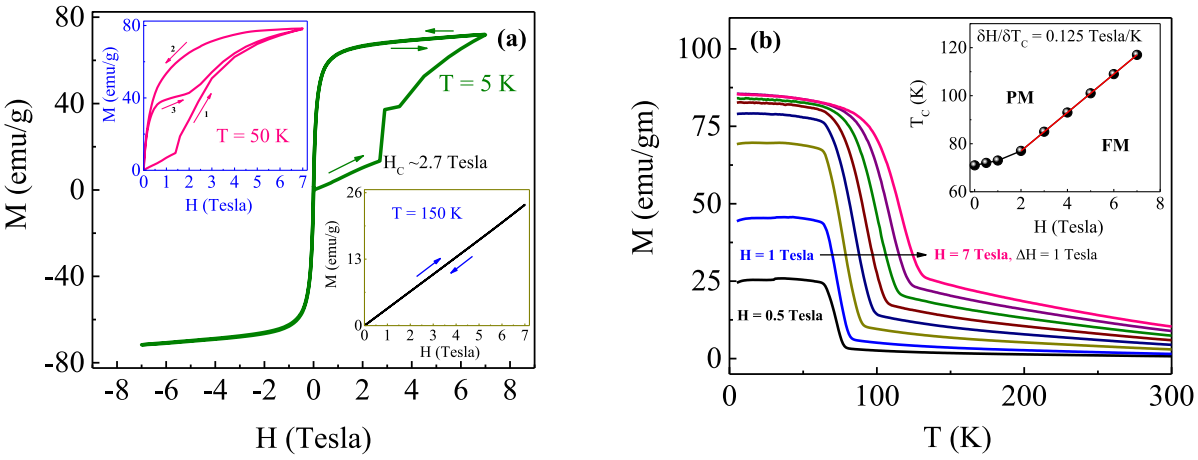


**Fig. 2.** (a) Isothermal magnetization (M–H) data recorded at $T$ = 5 K (main panel), 50 K (upper inset) and 150 K (lower inset) for the desired quadrants, (b) Isofield magnetization measurements (M–T) recorded for various external magnetic fields under field-cooled-warming protocol. The inset shows the magnetic phase diagram ($T_C$ - H) constructed from the isofield magnetization data.

field hysteresis with its complete linear nature in the M–H curve at $T$ = 150 K represents the conversion of mixed-phase state (AFM + FM) into paramagnetic (PM) one. This whole process can be well understood from the scenario of martensitic-like phase transition [47,70].

The temperature dependence of magnetization measurements have been carried out for various external magnetic fields as shown in Fig. 2(b). Here we must mention that before each measurement, the sample was cooled down to the lowest temperature in the presence of desired static magnetic field and data were recorded during the warming cycle in the presence of the same static magnetic field as applied during cooling the system. With decreasing temperature, the FM volume phase fraction started to grow. As a result, magnetization increases accordingly. A sudden jump in the value of magnetization has been noticed in the vicinity of the transition temperature, $T_C$ and the system converted into a PM one [71]. With the application of magnetic fields, the transition temperature, $T_C$ starts to shift towards higher temperature linearly at the rate of 0.125 Tesla/K as shown in the magnetic phase diagram in the inset of Fig. 2(b).

The conventional super-exchange and double exchange interaction models where all the oxygen anions were assumed as negative divalent ions in the oxide compounds can be used to understand the underlying physics behind this phenomenon [72,73]. From the magnetization as a function of temperature data (Fig. 2(b)), another prominent transition is also observed at the very low temperature (T < 50 K). However, in the presence of large external magnetic field, the signature was diminished. Such transition was also reported earlier in case of similar types of other manganite compounds [73–75]. The transition at the low temperature can be explained using the itinerant electron model for magnetic oxide (IEO) as reported by Tang et al. [73]. According to their model, different ionic valencies in the polycrystalline compounds play crucial role for magnetic ordering especially at the low temperature region [73,76–78]. Additionally, the interactions of various magnetically canted sublattices (constituted by rare-earth and Mn-ions) corroborates such prominent magnetic transition at the low temperature region.

To get the clear picture of the high-temperature PM state, the reciprocal of susceptibility, $\chi^{-1}$ as a function of temperature for H = 0.05 Tesla has been plotted as shown in Fig. 3. The plot shows a non-linear behavior except the high temperature PM region. In that region, we used Curie–Weiss (CW) law of the form $\chi = C/(T - \theta_{CW})$, where $C = \mu_{eff}^2/3k$ is the Curie constant and $\theta_{CW}$ is the Weiss temperature. The linear fitting of the $\chi^{-1}$ vs. T plot results in a positive value of $\theta_{CW} \sim 123$ K, and an effective magnetic moment, $(\mu_{eff})_{exp} = 6.54\ \mu_B$/f.u.. One can calculate the value of effective magnetic moment theoretically using the formula, $(\mu_{eff})_{theo} = (0.5(\mu_{eff})^2_{Sm^{3+}} + 0.5(\mu_{eff})^2_{Mn^{3+}} + 0.5(\mu_{eff})^2_{Mn^{4+}})^{1/2}$; where, $(\mu_{eff})_{Sm^{3+}}$, $(\mu_{eff})_{Mn^{3+}}$ and $(\mu_{eff})_{Mn^{4+}}$ are calculated with the help of $\mu_{eff} = g\sqrt{j(j+1)}\mu_B$ formula. The as calculated effective magnetic moment, $(\mu_{eff})_{theo}$ = 4.45 $\mu_B$/ f. u. is lower than that of experimentally calculated value. Both the higher value of effective magnetic moment ($(\mu_{eff})_{exp}$) and positive value of $\theta_{CW}$ confirms the presence of short-range ordered FM clusters in the PM matrix of the compound [47].

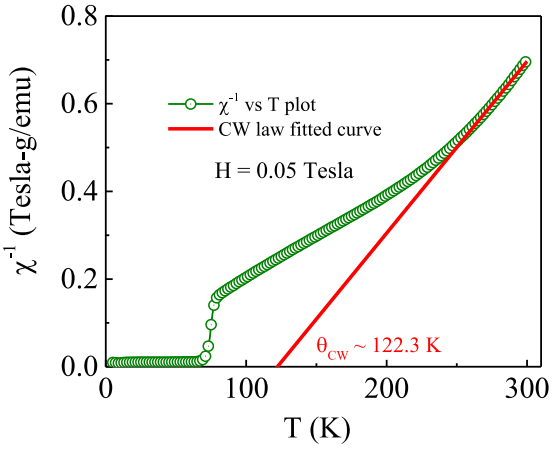


**Fig. 3.** Temperature dependence of the reciprocal of susceptibility ($\chi^{-1}$) along with the high-temperature Curie–Weiss law fitted curve.

### 3.3. Magnetocaloric effect (MCE)

To estimate the change of magnetic entropy ($\Delta S$) of the present studied SCSMO system using classical MR as given in Eq. (1), a set of isothermal magnetization curves have been recorded around a large temperature span of 10 K → 200 K with desired temperature interval of 5 K and 10 K with a maximum field change of 7 Tesla, presented in Fig. 4(a). The compound exhibits pronounced meta-magnetic-like transition at the low-temperature values. One can observe the two steps jumps of magnetization with the increasing magnetic field at $T$ = 10 K as presented by the dark solid black line in the respective figure. The values of the required critical magnetic field for the meta-magnetic-like transition reduces successively with increasing the temperature and the magnetization tends to saturate at the high field regions, indicating almost the complete melting of CO-AFM ground state into field-induced FM state. With increasing temperature, the thermal energy of the

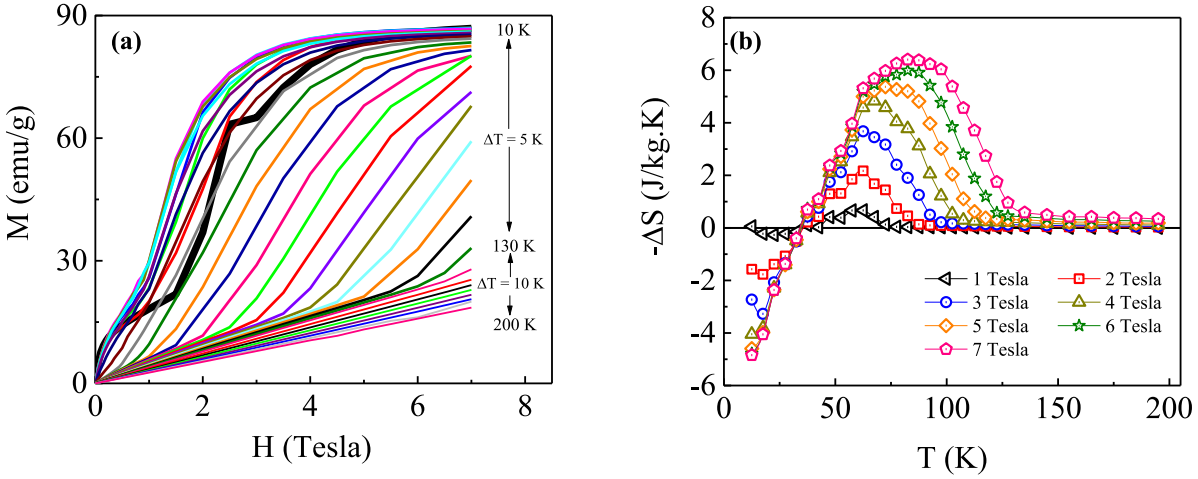


**Fig. 4.** (a) Isothermal magnetization curves recorded over wide range of temperature, $T$ = 10 K → 200 K upon field sweeping of 0 Tesla → 7 Tesla, (b) Isothermal magnetic entropy change ($-\Delta S$) as a function of temperature for various magnetic fields calculated using the Maxwell's relation.

system helps to loose the blockage of magnetic spins, resulting a PM ground state in the system [47]. The isothermal magnetization curves also indicate that there are the canted magnetic coupling (i) in between Mn–Mn sublattices and (ii) in between Sm–Sm sublattices. The canting angle increases with the increasing of the test temperature, resulting in the magnetization increases more slowly with more higher test temperatures.

One can conclude from the above discussion that the virgin system initially possesses a canted-type AFM ground state, which can be easily transformed into an FM irreversible and stable state upon application of a suitable amount of magnetic field. The presence of such metastable AFM ground state initiates irregular nature in the temperature dependence of magnetic entropy change curves ($-\Delta S$ vs. T), coined as the inverse magnetocaloric effect. We have plotted the variation of $-\Delta S$ with temperature under various external magnetic fields in Fig. 4(b). Below T ≤ 35 K, the compound exhibits negative values of $-\Delta S$ irrespective of the applied magnetic fields, pointing towards the inert AFM ground state of the compound. Although, we have claimed in the previous paragraph about the complete conversion of AFM state into FM one at high field regions, but the $-\Delta S$ vs. T curves indicate the presence of short-range AFM components at the low-temperature region independent even of 7 Tesla high magnetic field. A crossover of $-\Delta S$ from negative to positive values with increasing temperature along with a board distinct peak signifies the establishment of FM phase in the system. The FM transition temperature, $T_C$ represented by the peak temperature of $-\Delta S$ vs. T curves are shifting towards higher temperatures with increasing magnetic field values. The maximum value of magnetic entropy change ($\Delta S$) is found to be 6.4 J/kg K for a field change of 0 Tesla–7 Tesla. The compound also manifests the FOPT confirmed from the construction of Arrott's plot ($M^2$ vs. H/M) [79], which is not shown herewith.

In order to estimate the entropy change ($-\Delta S$) from the isofield magnetization data, the applicability of CC equation can be considered as one of the best methods. We are interested in the FM section of the entropy change ($-\Delta S$). For this purpose, we consider the M–T curves recorded in the field-cooled-warming (FCW) protocol for different external magnetic fields as shown in Fig. 2(b), where the system converted its ground state phase from FM to PM with decreasing temperature whatever be the applied magnetic fields. The reason behind to choose FCW M(T) curves is to avoid the thermal hysteresis as the compound shows a huge thermal hysteresis in between field-cooled-cooling (FCC) and FCW M–T curves as discussed in our earlier reports [33]. The FM phase fraction of magnetization, f(T) of the system can be estimated by assuming the fact that the total magnetization is directly proportional to the phase volume fraction [48,49]. To estimate

**Table 3**
Magnetocaloric parameters of single-crystalline SCSMO compound. Here MR stands for Maxwell's relation and CC stands for Clausius–Clapeyron equation.

| H | $\Delta S_{max}$ (J/kg K) | | RCP (J/kg) | | $\Delta T_{ad}$ |
|---|---|---|---|---|---|
| (Tesla) | MR | CC | MR | CC | (K) |
| 1 | 0.66 | 0.79 | 15.58 | 5.79 | 0.37 |
| 2 | 2.17 | 2.90 | 62.81 | 33.46 | 0.71 |
| 3 | 3.67 | 5.05 | 123.92 | 79.46 | 1.56 |
| 4 | 4.58 | 6.19 | 189.56 | 136.30 | 2.21 |
| 5 | 5.36 | 6.53 | 259.53 | 184.92 | 2.56 |
| 6 | 5.99 | 6.43 | 318.01 | 222.61 | 2.78 |
| 7 | 6.40 | 6.14 | 386.88 | 257.63 | 2.94 |

the value of f(T) for various magnetic fields, it is requisite to obtain the magnetization data of both the pure FM phase ($M_{FM}$) and fully PM phase ($M_{PM}$) for a constant temperature. As a result, linear extrapolation of M–T data in the two different phases have been employed to get the $M_{FM}$ and $M_{PM}$ data which are presented by blue and olive solid lines in Fig. 5(a) respectively. Using M(T), $M_{FM}$(T) and $M_{PM}$(T) data, one can estimate the normalized FM phase fraction, f(T) by using the expression,

$$f(T) = \frac{M(T) - M_{PM}}{M_{FM} - M_{PM}} \times 100\% \quad (3)$$

The normalized f(T) curve with respect to temperature is plotted by the pink solid line for a field change of H = 4 Tesla as a representation as shown in Fig. 5. It is reported in the literature that the impact of both temperature and magnetic field is thermodynamically equivalent as an operating force for the change of magnetic phases. To confirm the fact, we have calculated f(T) for different magnetic fields from the M–T data (from Fig. 2(b)) and presented in Fig. 5(b). The nature of the f(T) curves remain unchanged irrespective of the applied fields and the respected phase transition temperature, $T_C$ is shifting towards the higher temperature with increasing magnetic field values like the M(T) curves. The transition temperature, $T_C$ increases with increasing the field values at the rate of 8 K/Tesla. The net change of f(T) with the increasing magnetic field can be calculated by using the following equation,

$$\Delta f(T, \Delta H) = f(T, H_f) - f(T, H_i) \quad (4)$$

where $H_i$ and $H_f$ are the initial and final values of the magnetic field respectively [48]. In our case, we consider 0.5 Tesla as the initial field value to calculate $\Delta$f(T, $\Delta$H). The variation of $\Delta$f(T, $\Delta$H) with temperature for different field values is shown in the inset of Fig. 5 (b).

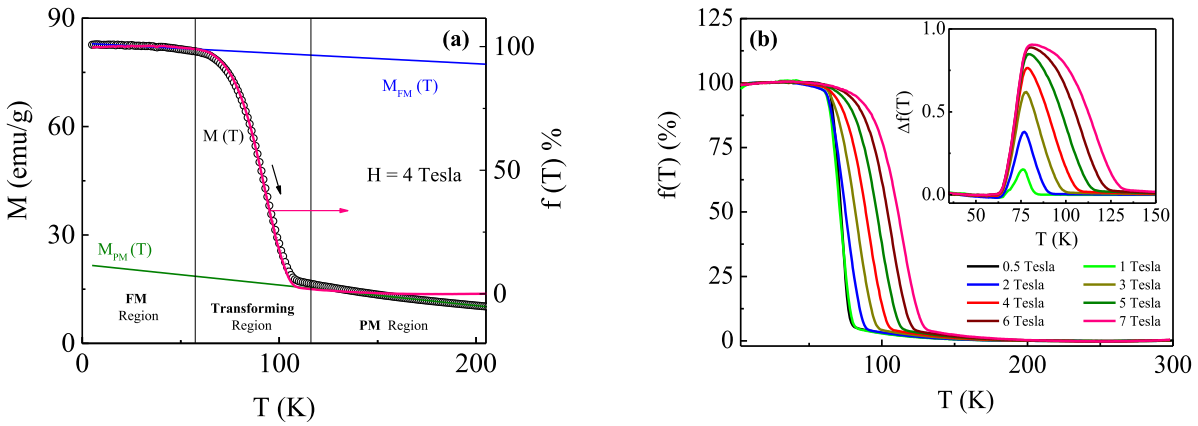


**Fig. 5.** (a) Magnetization as a function of temperature represented by black open circles measured at H = 4 Tesla. The blue and olive solid lines represent the extrapolated ferromagnetic ($M_{FM}$) and paramagnetic ($M_{PM}$) magnetization data respectively. The equivalent ferromagnetic phase fraction, f(T) is presented by using a solid pink line, (b) Variation of normalized ferromagnetic phase fraction, f(T) with temperature calculated for various magnetic fields. Inset shows the corresponding Δf(T) versus T curves estimated from the f(T) curves. (For interpretation of the references to color in this figure legend, the reader is referred to the web version of this article.)

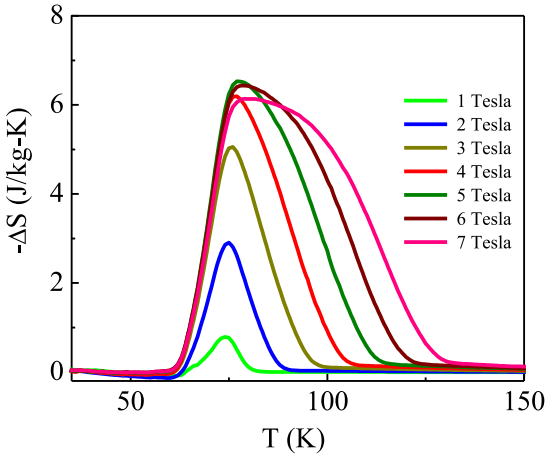


**Fig. 6.** Variation of isothermal magnetic entropy change (-ΔS) as a function of temperature calculated by using the Clausius–Clapeyron equation.

For a complete transformation of a pure FM phase into a pure an PM phase, and vice versa, the total entropy change (ΔS) in the vicinity of the magnetic phase transition region can be quantitatively calculated using the CC equation as given in Eq. (2). Since the tendency of phase transformation is directly affected by the magnetic field, one has to modify the CC equation of the following form [48] by considering the value of Δf(T, ΔH),

$$\Delta S = -\Delta f . \Delta M \left(\frac{dT_c}{dH}\right)^{-1} \quad (5)$$

where, ΔM = $M_{FM}$ - $M_{PM}$ is the difference of magnetization in between pure FM state and PM state. The variation of as the calculated entropy change (−ΔS) using the above expression with temperature for the field change from H = 1 Tesla to 7 Tesla are shown in Fig. 6. The pattern of the −ΔS vs. T curves are almost similar to that of the obtained curves using MR (shown in Fig. 4(b)). The maximum value of the entropy change slightly decreases from 6.53 J/kg K (ΔH ≃ 5 Tesla) to 6.14 J/kg K (ΔH ≃ 7 Tesla). The reason behind such an interesting result may be due to the decreasing of net values of Δf(T, ΔH) in the high field values. Regarding this context, we must mention that not a single spurious spike has been observed in the −ΔS vs. T curves calculated from both the methods. Table 3 shows the comparison of the maximum values of entropy change ($|\Delta S_{max}|$) calculated using MR and CC equation for the various applied magnetic fields.

**Table 4**
Comparison of magnetocaloric parameters ($\Delta S_{max}$ and RCP) of the present studied systems along with some other oxide compounds.

| Compounds | $\Delta S_{max}$ (J/kg K) | H (Tesla) | RCP (J/kg) | References |
|---|---|---|---|---|
| SCSMO | 5.36 | 5 | 260 | Present work |
| $La_{0.67}Sr_{0.33}Mn_{0.9}Cr_{0.1}O_3$ | 5.00 | 5 | 200 | [81,82] |
| $La_{0.7}Ca_{0.05}Sr_{0.25}MnO_3$ | 6.86 | 5 | 364 | [81,83] |
| $La_{0.67}Ba_{0.33}MnO_3$ | 1.48 | 5 | 161 | [81,84] |
| $La_{0.67}Sr_{0.33}MnO_3$ | 1.69 | 5 | 211 | [81,84] |
| $La_{0.67}Ca_{0.33}MnO_3$ | 2.06 | 5 | 175 | [81,84] |
| $La_{0.87}Sr_{0.13}MnO_3$ | 5.80 | 5 | 232 | [81,85] |
| $La_{0.84}Sr_{0.16}MnO_3$ | 5.85 | 5 | 240 | [81,85] |
| $GdMnO_3$ | 15 | 7 | 211 | [86] |
| $GdAlO_3$ | 3.4 | 7 | 203 | [86] |

To understand the quality of any magnetic refrigerant material, RCP is more frequently used by researchers [80]. It is defined as the net change of heat transfer between a hot source and a cold reservoir in an ideal refrigerant cycle of any magnetic refrigerant material [80]. RCP can be quantified as the product of maximum values of entropy change, $|\Delta S_{max}|$ and the full width at half maxima of the temperature, $\delta T_{FWHM}$ of −ΔS vs. T curve i.e. RCP = $|\Delta S_{max}| \times \delta T_{FWHM}$. Higher values of RCP can be achieved either by getting a large value of $|\Delta S_{max}|$ or widespread of −ΔS vs. T curves and sometimes both the possibilities are considered as much suitable option. We have calculated the RCP from both the −ΔS vs. T curves obtained by using MR and CC equation and compare their values along with the $|\Delta S_{max}|$ in Table 3 for different field values. Table 4 also presents a comparison of the magnetocaloric parameters (both $|\Delta S_{max}|$ and RCP) of the present studied system along with some other similar types of manganite compounds.

To ensure the potentiality of a magnetic refrigerant material, apart from the value of $|\Delta S_{max}|$ and RCP, another parameter, named as adiabatic temperature change, $\Delta T_{ad}$ is widely used worldwide. $\Delta T_{ad}$ is defined as the isentropic temperature difference between S(H, T) and S(0, T). Alternatively, one can estimate the $\Delta T_{ad}$ using the classical MR of the form

$$\Delta T_{ad}(T, H) = -\int_0^H \frac{T}{C_P}\left(\frac{\partial M}{\partial T}\right) dH \quad (6)$$

where $C_P$ is the heat capacity of the system in the absence of a magnetic field. We follow the first method to estimate the value of $\Delta T_{ad}$. For that at first, we calculate the total entropy of the system in absence of magnetic field, S(0, T) from the zero-field heat capacity data which will be discussed in the next section. The total entropy in the presence of various magnetic fields can be obtained from the addition of S (0,

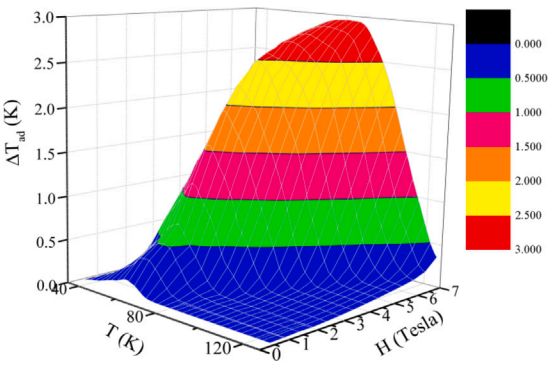


**Fig. 7.** The 3D contour plot of $\Delta T_{ad}$ as a function of both temperature and magnetic field obtained from the isothermal magnetization measurements and zero-field heat capacity data.

T) and $-\Delta S$ calculated from isothermal magnetization measurements. The $\Delta T_{ad}$ can be calculated from the relation $\Delta T_{ad}$ = [T(S, H) - T(S, 0)]$_{S=constant}$. We have used the values of entropy change, $\Delta S$ calculated using MR and considering only the positive part of the $-\Delta S$ vs. T curves above T ≥ 30 K. The as calculated $\Delta T_{ad}$ for various applied magnetic fields and its variation along with the temperature is shown as a 3D contour plot in Fig. 7. The obtained maximum values of $\Delta T_{ad}$ for this studied system is also presented in Table 3.

### 3.4. Heat capacity measurements

In order to get a better insight into the phenomenon that takes place in the studied SCSMO system, we have measured the heat capacity ($C_P$) in the temperature range of 2 K–302 K without any magnetic field. The temperature dependence of zero-field heat capacity ($C_P$) data is presented in the main panel of Fig. 8(a). The value of $C_P$ increases progressively above $T$ = 10 K with increasing temperature and it approaches the value of about 108.7 J/ mol K at $T$ = 302 K. According to the Dulong–Petit law, the classical limit of $C_P$ at high temperature is estimated by using the expression $C_P$ = 3nR, where n is the number of atoms per unit cell and R is the universal gas constant. The highest observed experimental value of $C_P$ is just 87% of the theoretically predicted value of $C_P \simeq$ 125 J/kg K for n = 5. In the temperature range between $T$ = 10 K–302 K, no strong anomaly due to any local ordering has been noticed. Below T < 10 K, a prominent shoulder peak in the heat capacity data has been observed. This board hump around $T_S$ = 7.52 K may be associated with a Schottky-like anomaly caused by the crystal-field level excitations of unpaired 4f electronic states of $Sm^{3+}$ ions [87]. A similar type of Schottky-like anomaly is also reported for the $Sm_{0.5}Ca_{0.5}MnO_3$ compound [28]. For better understanding the $C_P$ data, we have divided and analyzed the data in two different temperature regions namely low temperature Schottky-like anomaly region and the classical high temperature region.

Various factors influence the $C_P$ of any system and to analyze the $C_P$ vs. T data, contributions from different sources must be accounted for. In the high-temperature region, phonon-lattice contribution becomes the dominating factor in the $C_P$ data. The studied SCSMO system shows highly insulating behavior due to the localization of $e_g$ conduction electrons down to the lowest measurable temperature. Therefore, the electronic contribution of the $C_P$ ($C_{elec}$) does not account in the present study ($C_{elec}$ = 0) [28]. The Debye-model of $C_P$ of the following form has been used to extract the lattice contribution of the $C_P$ from the total $C_P$ data,

$$C_{lat} = 9nR\left(\frac{T}{\Theta_D}\right)^3 \int_0^{\Theta_D/T} \frac{x^4 e^x}{(e^x-1)^2} dx \quad (7)$$

where $\Theta_D$ is the Debye temperature and x = $\hbar\omega/k_BT$ (symbols have their usual meanings). The zero-field $C_P$ data along with the Debye

**Table 5**
The extracted Schottky parameters obtained from the Schottky-like anomaly fitting of the low-temperature zero-field heat capacity data.

| $T_S$ (K) | $\omega_1$ | $\omega_2$ | $\omega_3$ | $\sum\omega_N$ | $\Delta_1$ (meV) | $\Delta_2$ (meV) | $\Delta_3$ (meV) | $\Delta_3$ - $\Delta_1$ (meV) |
|---|---|---|---|---|---|---|---|---|
| 7.52 | 0.266 | 0.371 | 0.400 | 1.037 | 0.46 | 0.95 | 1.93 | 1.47 |

model fitted curve in the high-temperature region is displayed in the main panel of Fig. 8(a) by solid black spheres and solid red line respectively. The obtained value of the $\Theta_D$ is around 517 K. However, below T = 100 K, the fitted curve strongly deviates from the experimental data points. This may be attributed to the fact that, below $T$ = 100 K, other contributions like magnetic, hyperfine, crystal-field splitting, etc. start to dominant over the lattice contribution [88]. The magnetic contribution of the $C_P$ ($C_{mag}$) is extracted from the total heat capacity, $C_{total}$ after the subtraction of the lattice part, $C_{lat}$ of the $C_P$ data i.e. $C_{mag}$ = $C_{total}$ - $C_{lat}$. The extracted magnetic curve of $C_P$ ($C_{mag}$) is shown in the main panel of Fig. 8(a) by solid olive line. A strong board hump in the $C_{mag}$ curve has been noticed at around T ≈ 55 K, which is very close to the value of $T_C$ of the studied system [33]. The associated magnetic entropy, $S_{mag}$ can be estimated using the given formula,

$$S_{mag} = \int_{T_1}^{T_2} \frac{C_{mag}}{T} dT \quad (8)$$

The variation of $S_{mag}$ with temperature is shown in the inset of Fig. 8(a). $S_{mag}$ reaches the saturation value of 1.44R just above T = 100 K. This zero-field magnetic entropy ($S_{mag}$) has been used to evaluate the adiabatic temperature change ($\Delta T_{ad}$) as mentioned in the last section. At zero field, the estimated saturation value of $S_{mag}$ = 1.497R if we only consider the contribution of 50% $Mn^{3+}$ ions and 50% from $Mn^{4+}$ ions to the total $C_P$. Upon consideration of $Sm^{3+}$ ions contribution to the total $C_P$, the total estimated released entropy would be 2.392R whose 60% value is close to the experimentally obtained value of entropy. On the other hand, an excellent agreement in the values of $S_{mag}$ has been observed (~ 96%) if we consider the contribution only from Mn-ions. This kind of discernible result in magnetic entropy has also been found in other manganite system [88–90].

The temperature window (2 K, 42 K) has been used to understand the low temperature Schottky-like anomaly in the $C_P$ data. Apart from the significant shoulder at around 7.5 K, higher values of $C_P$ have been noticed in the low-temperature region that is one order of magnitude higher than that of some other reported manganite systems [91,92]. Due to the localization of charge carriers in the CO state, the effective mass of the charge carriers increases, and as a result higher values of $C_P$ have been observed at low temperatures. This is also the reason behind not including the linear electronic contribution term of $C_P$ in the analysis. In addition to that, the hyperfine contribution to the specific heat with a $T^{-2}$ dependence term, caused by the local magnetic field at the Sm and Mn nuclei is negligible at T ≥ 2 K [93]. Therefore, the final expression for the total heat capacity at low temperature region with a Schottky-term ($C_{sch}$) can be expressed as

$$C_{total} = C_{lat} + C_{mag} + C_{sch} \quad (9)$$

where the first term, $C_{lat}$ represent the lattice contribution [30] in the $C_P$ and can be expressed as $C_{lat} = \sum\beta_{2n+1}T^{2n+1}$. The parameters $\beta_{2n+1}$ (n = 1, 2, 3, ….) represent the contribution of phonon nodes. The first term of phonon nodes, $\beta_3$ is related to the Debye temperature ($\Theta_D$) of the system in the low-temperature region. Higher values of n have been used to well fit the data at the high-temperature limit. We have used n = 3 to get the best fit of the $C_P$ data points up to $T$ = 42 K. The second magnetic term, $C_{mag} = \delta T^n$, n > 0 is used to extract any information regarding spin-waves of the system. The parameter $\delta$ is related to stiffness-constant of spin-waves. It is proposed that the value of n should be 1.5, 2 and 3 for an FM, layered AFM, and isotropic AFM system respectively [94]. In our case, we set the parameter n free

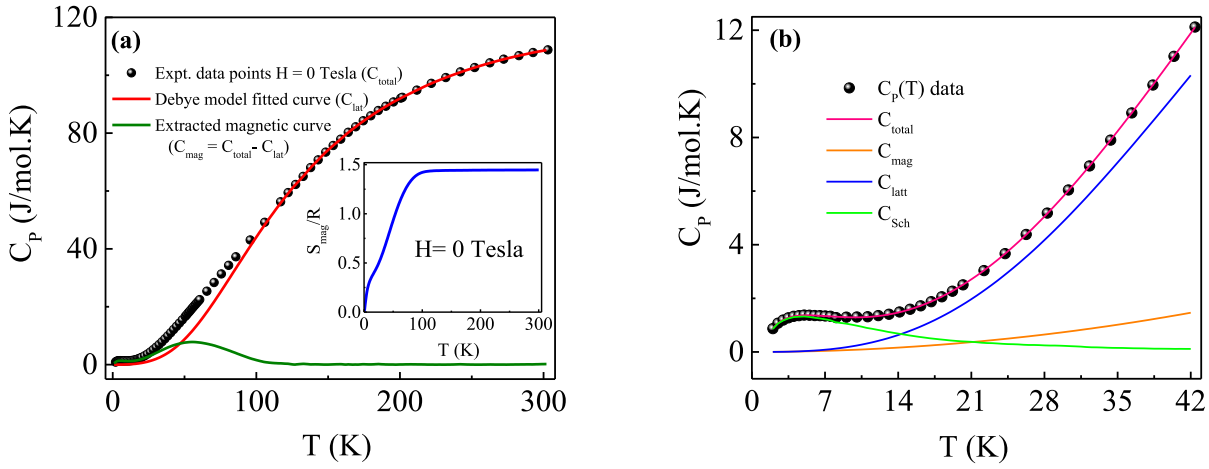


**Fig. 8.** (a) Temperature dependence of the zero-field heat capacity ($C_P$) dta along with the Debye model fitted curve represented by the red line of the SCSMO single crystal. The magnetic contribution ($C_{mag}$) of the heat capacity is represented by the solid olive line in the same figure. Inset shows the temperature dependence of the zero-field magnetic entropy ($S_{mag}$) of the SCSMO compound, (b) Low-temperature zero-field heat capacity along with the fitted curve according to Eq. (9) and the respective contributions to low-temperature heat capacity are also presented individually in the same figure. (For interpretation of the references to color in this figure legend, the reader is referred to the web version of this article.)

during the fitting of low-temperature $C_P$ vs. T data. The best-fitting has been obtained for the value of n close to 2, suggests the dominant AFM ground state of the system. Finally, the Schottky contribution ($C_{sch}$) to the $C_P$ is described by a discrete distribution of $N_S$ two-level systems having different splitting energies, $\Delta_i$ of the ground state doublet of $Sm^{3+}$ ion corresponding to different weight factors, $\omega_i$. The expression for the $C_P$ due to Schottky-like anomaly [87,95] can be expressed as

$$C_{sch} = \frac{1}{2}R\sum_{i=1}^{N_S}\omega_i\frac{(\frac{\Delta_i}{k_BT})^2 exp(\frac{\Delta_i}{k_BT})}{[1+exp(\frac{\Delta_i}{k_BT})]^2} \quad (10)$$

$$\sum_{i=1}^{N_S}\omega_i = 1$$

During the fitting, we have used both single and double Schottky levels individually to obtain the best version of the fitting of the experimental data points. But the fitting did not improve in either cases. It is reported in the literature that in a crystal field of low symmetry, $Sm^{3+}$ ion would be expected to split into three doublet levels [96]. We have used three Schottky levels ($N_S = 3$) to fit the data points and a strong correlation between Schottky energy levels ($\Delta_i$) has been observed. The final fitted curve ($C_{total}$) along with the experimental data points is shown in Fig. 8(b). The goodness of fitting can be judged by the obtained value of reduced $\chi^2 = 1.139 \times 10^{-4}$. Different contributions to the total $C_P$ at the low-temperature have been extracted from the fitted curve which are plotted in the same figure of Fig. 8(b). The results of our Schottky approximations are summarized in Table 5. The energy difference $\Delta_3$ - $\Delta_1$ = 1.47 meV is nearly matching with that of other CO manganite systems [93,95,97].

From the first phonon mode, $\beta_3$, the Debye temperature, $\Theta_D$ [87] can be calculated using the following expression

$$\Theta_D = \left(\frac{12\pi^4 nR}{5\beta_3}\right)^{\frac{1}{3}} \quad (11)$$

The obtained value of $\Theta_D$ is 340.8 K and this value is in good agreement with that of the obtained values for similar types of manganite systems [87,88,98]. Here we must mention that at high temperature above T > 20 K, the $C_P$ data is strongly dominated by the lattice contributions ($C_{lat}$) with its higher-order term ($\beta_5 T^5 + \beta_7 T^7$). For a two-level Schottky function, the energy splitting ($\Delta_i$) could also be related to the peak temperature ($T_S$) of the Schottky peak [30] in the specific heat by the relation, $\Delta = k_B T_S/0.418$. The as obtained value of energy splitting 1.55 meV is well-matched with that of obtained from the Schottky fitting parameter (1.47 meV). Due to the lack of information about the low temperature $C_P$ data of Sm based manganite systems, we are free to compare our result for similar kind of manganite system. As already mentioned above, our experimental results are well-grounded and authentic for perovskite manganite systems.

## 4. Conclusions

In summary, we have carried out detail investigation on the magnetic and magnetocaloric properties of single-crystalline SCSMO compound through both isothermal and isofield magnetization measurements as well as heat capacity measurement. X-ray photoelectron spectroscopy study reveals that the almost equal distribution of $Mn^{3+}$ and $Mn^{4+}$ ions in the studied system which is an essential criterion for a manganite material having charge-ordered state. The core-level binding energy spectra of O-1s can be well-descried with three simulated curves with respect to the three different binding energies. These three fitted peaks can be ascribed as $O^{2-}$ ions at 529.06 eV, $O^{1-}$ ions at 531.29 eV, and chemically adsorbed oxygens, $O^{chem}$ at 533.24 eV. We have also estimated the average valence of oxygen ions ($V_{aO^-}$) and net oxygen content ($\delta$) in the present system. The appropriate proportions of the $Mn^{3+}$ and $Mn^{4+}$ ions is also reflected in the magnetic measurements of the compound. The isothermal magnetization measurement at low temperature discloses the presence of field-induced meta-magnetic-type transition in the system. This interesting phenomenon could result in an inverse magnetocaloric effect at T ≤ 35 K calculated using Maxwell's relation. We have also estimated the magnetic entropy change by utilizing the modified Clausius–Clapeyron equation. Our experimental findings help to deal with the phenomenon related with the magnetocaloric effect for many magnetic systems having the first-order magnetic phase transition. No strong anomaly has been observed in the zero-field heat capacity data down to 20 K from 302 K. Presence of a board Schottky-like anomaly has been noted in the low temperature (2 K < T < 20 K) heat capacity data. This Schottky-like anomaly is treated with a sum of three two-levels Schottky functions along with the consideration of both lattice-phonon and AFM spin-wave contributions. Owing to the localization of charge carriers, higher values of heat capacity at low temperature has been achieved which further confirms the dominating charge-ordered AFM ground state of the compound. The present results of the studied SCSMO compound are overall persistent with similar types of charge-ordered manganite compounds.

## Declaration of competing interest

The authors declare that they have no known competing financial interests or personal relationships that could have appeared to influence the work reported in this paper.

## Acknowledgments

The work was supported by the Department of Atomic Energy (DAE), Govt. of India. The authors would like to thank Prof. K. S. R. Menon and Mr. Arunava Kar of SINP for helping in performing the XPS measurements and analysis. The authors would also like to acknowledge UGC-DAE Consortium for Scientific Research, Indore center, India for performing heat capacity measurements.

## References

[1] M.B. Salamon, M. Jaime, Rev. Modern Phys. 73 (2001) 583.
[2] Y. Tokura, Colossal Magnetoresistive Oxides, Gordon and Breach Science Publishers, The Netherlands, 2000.
[3] E. Dagotto, Science 309 (2005) 257;
N. Mathur, P. Littlewood, Phys. Today 56 (1) (2003) 25.
[4] A. Asamitsu, Y. Tomioka, H. Kuwahara, Y. Tokura, Nature 388 (1997) 50.
[5] A. Sawa, Mater. Today 11 (2008) 28.
[6] D. Rubi, F. Tesler, I. Alposta, A. Kalstein, N. Ghenzi, F. Gomez-Marlasca1, M. Rozenberg, P. Levy, Appl. Phys. Lett. 103 (2013) 163506.
[7] M. Bibes, A. Bathelemy, IEEE Trans. Electron Devices 54 (2007) 1003.
[8] T. Hotta, M. Moraghebi, A. Feiguin, A. Moreo, S. Yunoki, Elbio Dagotto, Phys. Rev. Lett. 90 (2003) 247203.
[9] J.S. Zhou, J.B. Goodenough, J.M. Gallardo-Amores, E. Moran, M.A. Alario-Franco, R. Caudillo, Phys. Rev. B 74 (2006) 014422.
[10] S. Dong, R. Yu, S. Yunoki, J.M. Liu, E. Dagotto, Phys. Rev. B 78 (2008) 155121.
[11] S. Jin, T.H. Tiefel, M. McCormack, R.A. Fastnacht, R. Ramesh, L.H. Chen, Science 264 (1994) 413.
[12] M. Baldinia, T. Muramatsub, M. Sherafatic, H. Maob, L. Malavasie, P. Postorinog, S. Satpathyh, V.V. Struzhkin, Proc. Natl. Acad. Sci. USA 112 (2015) 10869.
[13] J. Salafranca, L. Brey, Phys. Rev. B 73 (2006) 024422.
[14] Z.B. Guo, Y.W. Du, J.S. Zhu, H. Huang, W.P. Ding, D. Feng, Phys. Rev. Lett. 78 (1997) 1142.
[15] K.A. Gschneidner Jr., V.K. Pecharsky, A.O. Tsokol, Rep. Progr. Phys. 68 (2005) 1479.
[16] R.Y. Gu, C.S. Ting, Phys. Rev. B 65 (2002) 214426.
[17] P. Debye, Ann. Physics 81 (1926) 1154;
W.F. Giauque, J. Am. Chem. Soc. 49 (1927) 1864.
[18] Y. Tomioka, Y. Tokura, Phys. Rev. B 70 (2004) 014432.
[19] N.A. Babushkina, E.A. Chistotina, O.Yu. Gorbenko, A.R. Kaul, D.I. Khomski, K.I. Kugel, Phys. Rev. B 67 (2003) 100410(R).
[20] Y. Endoh, H. Hiraka, Y. Tomioka, Y. Tokura, N. Nagaosa, T. Fujiwara, Phys. Rev. Lett. 94 (2005) 017206.
[21] D. Mazumdar, K. Das, I. Das, J. Appl. Phys. 127 (2020) 093902.
[22] L.E. Gonchar, A.E. Nikiforov, Phys. Rev. B 88 (2013) 094401.
[23] S. Chattopadhyay, S. Giri, S. Majumdar, J. Appl. Phys. 112 (2012) 083915.
[24] N.T.M. Duc, C.M. Hung, N.T. Huong, M.H. Phan, J. Electron. Mater. 49 (2020) 2596.
[25] J. Fan, W. Zhang, X. Zhang, L. Zhang, Y. Zhang, Mater. Chem. Phys. 144 (2014) 206.
[26] Y. Tokura, Y. Tomioka, J. Magn. Magn. Mater. 200 (1999) 1.
[27] E. Dagotto, Nanoscale Phase Separation and Colossal Magnetoresistance: The Physics of Manganites and Related Compounds, Springer, Berlin, 2003.
[28] D. Niebieskikwiat, M.B. Salamon, Phys. Rev. B 72 (2005) 174422.
[29] V. Podzorov, B.G. Kim, V. Kiryukhin, M.E. Gershenson, S.W. Cheong, Phys. Rev. B 64 (2001) 140406(R).
[30] J. Lopez, O.F. de Lima, P.N. Lisboa-Filho, F.M. Araujo-Moreira, Phys. Rev. B 66 (2002) 214402.
[31] H.D. Aliyu, J.M. Alonso, P. de la Presa, W.E. Pottker, B. Ita, M.G. Hernandez, A. Hernando, Chem. Mater. 30 (2018) 7138.
[32] O.S. Mantytskaya, I.O. Troyanchuk, A.N. Chobot, H. Szymczak, Low Temp. Phys. 30 (2004) 218.
[33] D. Mazumdar, K. Das, S. Roy, I. Das, J. Magn. Magn. Mater. 497 (2020) 166066.
[34] H. Yoshizawa, H. Kawano, Y. Tomioka, Y. Tokura, Phys. Rev. B 52 (1995) R13145.
[35] H.Y. Hwang, T.T.M. Palstra, S.W. Cheong, B. Batlogg, Phys. Rev. B 52 (1995) 15046.
[36] D. Mohan Radheep, P. Sarkar, S. Arumugam, P. Mandal, Appl. Phys. Lett. 102 (2013) 092406.
[37] V. Kiryukhin, D. Casa, J.P. Hill, B. Keimer, A. Vigliante, Y. Tomioka, Y. Tokura, Nature 386 (1997) 813.
[38] T. Hashimoto, T. Numasawa, M. Shino, T. Okada, Cryogenics 21 (1981) 647.
[39] R. Caballero-Flores, N.S. Bingham, M.H. Phan, M.A. Torija, C. Leighton, V. Franco, A. Conde, T.L. Phan, S.C. Yu, H. Srikanth, J. Phys.: Condens. Matter 26 (2014) 286001.
[40] M. Balli, O. Sari, D. Fruchart, J. Forchelet, EPJ Web Conf. 29 (2005) 00005.
[41] L. Caron, Z.Q. Oub, T.T. Nguyen, D.T. Cam Thanh, O. Tegus, E. Bruck, J. Magn. Magn. Mater. 321 (2009) 3559.
[42] G.J. Liu, J.R. Sun, J.Z. Wang, B.G. Shen, Appl. Phys. Lett. 89 (2006) 222503.
[43] A. Giguere, M. Foldeaki, B.R. Gopal, R. Chahine, T.K. Bose, A. Frydman, J.A. Barclay, Phys. Rev. Lett. 83 (1999) 2262.
[44] H. Wada, Y. Tanabe, Appl. Phys. Lett. 79 (2001) 3302.
[45] L. Tocado, E. Palacios, R. Burriel, J. Appl. Phys. 105 (2009) 093918.
[46] Z.G. Guo, L.Q. Pam, M.Y. Rafique, X.F. Zheng, H.M. Qiu, Z.H. Liu, J. Alloys Compd. 577 (2013) 174.
[47] D. Mazumdar, K. Das, I. Das, J. Magn. Magn. Mater. 502 (2020) 166507.
[48] K. Xu, Z. Li, Y.L. Zhang, C. Jing, Phys. Lett. A 379 (2015) 3149.
[49] Z. Li, Y. Zhang, K. Xu, T. Yang, C. Jing, H.L. Zhang, Solid State Commun. 203 (2015) 81.
[50] A. Arulraj, P.N. Santhosh, R.S. Gopalan, A. Guha, A.K. Raychaudhuri, N. Kumar, C.N.R. Rao, J. Phys. Condens. Matter 10 (1998) 8497.
[51] Y. Tokura, Y. Tomioka, J. Magn. Magn. Mater. 200 (1999) 1.
[52] Y. Tokura, Rep. Progr. Phys. 69 (2006) 797.
[53] S. Banik, K. Das, T. Paramanik, N.P. Lalla, B. Satpati, K. Pradhan, I. Das, NPG Asia Mater. 10 (2018) 923.
[54] P. Decorse, E. Quenneville, S. Poulin, M. Meunier, A. Yelon, F. Morin, J. Vac. Sci. Technol. A 19 (2001) 910.
[55] L.K. Joy, S.S. Samatham, S. Thomas, V. Ganesan, S. Al-Harthi, A. Liebig, M. Albrecht, M.R. Anantharaman, J. Appl. Phys. 116 (2014) 213701.
[56] U. Shankar, A.K. Singh, J. Phys. Chem. C 119 (2015) 28620.
[57] W. Xia, H. Wu, P. Xue, X. Zhu, Nanoscale Res. Lett. 13 (2018) 135.
[58] K. Das, I. Das, J. Appl. Phys. 119 (2016) 093903.
[59] E. Symianakis, D. Malko, E. Ahmad, A.S. Mamede, J.F. Paul, N. Harrison, A. Kucernak, J. Phys. Chem. C 119 (2015) 12209.
[60] L.Q. Wu, W.H. Qi, X.S. Ge, D.H. Ji, Z.Z. Li, G.D. Tang, W. Zhong, Eur. Phys. Lett. 120 (2017) 27001.
[61] E. Beyreuther, S. Grafstrom, L.M. Eng, C. Thiele, K. Dorr, Phys. Rev. B 73 (2006) 155425.
[62] J.J. Liang, H.-S. Weng, Ind. Eng. Chem. Res. 32 (1993) 2563.
[63] S. Jaiswar, K.D. Mandal, J. Phys. Chem. C 121 (2017) 19586.
[64] L.L. Ding, L.Q. Wu, X.S. Ge, Y.N. Du, J.J. Qian, G.D. Tang, W. Zhong, Results Phys. 9 (2018) 866.
[65] G. Panchal, D.K. Shukla, R.J. Choudhary, V.R. Reddy, D.M. Phase, J. Appl. Phys. 122 (2017) 085310.
[66] J.C. Dupin, D. Gonbeau, P. Vinatier, A. Levasseur, Phys. Chem. Chem. Phys. 2 (2000) 1319.
[67] L.Q. Wu, Y.C. Li, S.Q. Li, Z.Z. Li, G.D. Tang, W.H. Qi, L.C. Xue, X.S. Ge, L.L. Ding, AIP Adv. 5 (2015) 097210.
[68] L.Q. Wu, S.Q. Li, Y.C. Li, Z.Z. Li, G.D. Tang, W.H. Qi, L.C. Xue, L.L. Ding, X.S. Ge, Appl. Phys. Lett. 108 (2016) 021905.
[69] P. Sarkar, S. Arumugam, P. Mandal, A. Murugeswari, R. Thiyagarajan, S.E. Muthu, D.M. Radheep, C. Ganguli, K. Matsubayshi, Y. Uwatoko, Phys. Rev. Lett. 103 (2009) 057205.
[70] D.S. Rana, R. Nirmala, S.K. Malik, Europhys. Lett. 70 (3) (2005) 376.
[71] X.S. Ge, L.Q. Wu, S.Q. Li, Z.Z. Li, G.D. Tang, W.H. Qi, H.J. Zhou, L.C. Xue, L.L. Ding, AIP Adv. 7 (2017) 045302.
[72] A.S. Alexandrov, A.M. Bratkovsky, V.V. Kabanov, Phys. Rev. Lett. 96 (2006) 117003.
[73] G.D. Tang, Z.Z. Li, L. Ma, W.H. Qi, L.Q. Wu, X.S. Ge, G.H. Wu, F.X. Hu, Phys. Rep. 758 (2018) 1.
[74] X.S. Ge, L.Q. Wu, S.Q. Li, Z.Z. Li, G.D. Tang, W.H. Qi, H.J. Zhou, L.C. Xue, L.L. Ding, AIP Adv. 7 (2017) 045302.
[75] D.V. Maheswar Repaka, T.S. Tripathi, M. Aparnadevi, R. Mahendiran, J. Appl. Phys. 112 (2012) 123915.
[76] N. Niicker, J. Fink, J.C. Fuggle, P.J. Durham, W.M. Temmerman, Phys. Rev. B 37 (1988) 5158.
[77] H.L. Ju, H.-C. Sohn, K.M. Krishnan, Phys. Rev. Lett. 79 (1997) 3230.
[78] K. Ibrahim, H.J. Qian, X. Wu, M.I. Abbas, J.O. Wang, C.H. Hong, R. Su, J. Zhong, Y.H. Dong, Z.Y. Wu, L. Wei, D.C. Xian, Y.X. Li, G.J. Lapeyre, N. Mannella, C.S. Fadley, Y. Baba, Phys. Rev. B 70 (2004) 224433.
[79] A. Arrott, Phys. Rev. 108 (1957) 1394.
[80] K.A. Gschneidner Jr., V.K. Pecharsky, Annu. Rev. Mater. Sci. 30 (2000) 387.
[81] M.H. Phan, S.C. Yu, J. Magn. Magn. Mater. 308 (2007) 325.
[82] Y. Sun, W. Tong, Y.H. Zhang, J. Magn. Magn. Mater. 232 (2001) 205.
[83] M.H. Phan, S.C. Yu, N.H. Hur, Appl. Phys. Lett. 86 (2005) 072504.
[84] D.T. Morelli, A.M. Mance, J.V. Mantese, A.L. Micheli, J. Appl. Phys. 79 (1996) 373.
[85] A. Szewczyk, H. Szymczak, A. Wisniewski, K. Piotrowski, R. Kartaszynski, B. Dabrowski, S. Kolesnik, Z. Bukowski, Appl. Phys. Lett. 77 (2000) 1026.
[86] S. Mahana, U. Manju, D. Topwal, J. Phys. D: Appl. Phys. 50 (2017) 035002.
[87] S. Harikrishnan, C.M.N. Kumar, H.L. Bhat, S. Elizabeth, U.K. Robler, K. Dorr, S. Robler, S. Wirth, J. Phys.: Condens. Matter 20 (2008) 275234.

[88] M.R. Lees, O.A. Petrenko, G. Balakrishnan, D. McK. Paul, Phys. Rev. B 59 (1999) 1298.
[89] S. Robler, H.S. Nair, U.K. Robler, C.M.N. Kumar, S. Elizabeth, S. Wirth, Phys. Rev. B 84 (2011) 184422.
[90] A.P. Ramirez, P. Schiffer, S.W. Cheong, C.H. Chen, W. Bao, T.T.M. Palstra, P.L. Gammel, D.J. Bishop, B. Zegarski, Phys. Rev. Lett. 76 (1996) 3188.
[91] C.L. Lu, K.F. Wang, S. Dong, J.G. Wan, J.-M. Liu, Z.F. Ren, J. Appl. Phys. 103 (2008) 07F714.
[92] R.A. Fisher, F. Bouquet, N.E. Phillips, J.P. Franck, G.W. Zhang, J.E. Gordon, C. Marcenat, Phys. Rev. B 64 (2001) 134425.
[93] J.G. Cheng, Y. Sui, Z.N. Qian, Z.G. Liu, J.P. Miao, X.Q. Huang, Z. Lu, Y. Li, X.J. Wang, W.H. Su, Solid State Commun. 134 (2005) 381.
[94] V. Hardy, A. Wahl, C. Martin, Ch. Simon, Phys. Rev. B 63 (2001) 224403.
[95] E. Fertman, A. Beznosov, V. Desnenko, M. Kajnakova, A. Feher, J. Phys.: Conf. Ser. 150 (2009) 042031.
[96] B.H. Justice, E.F. Westrum Jr., J. Phys. Chem. 67 (1963) 659.
[97] B. Sattibabu, A.K. Bhatnagar, J. Therm. Anal. Calorim. 130 (3) (2017) 2015.
[98] J.J. Hamilton, E.L. Keatley, H.L. Ju, A.K. Raychaudhuri, V.N. Smolyaninova, R.L. Greene, Phys. Rev. B 54 (1996) 14926.